Title

Ethyl isopropyl amiloride decreases oxidative phosphorylation and increases mitochondrial fusion in clonal untransformed and cancer cells

Journal

American Journal of Physiology - Cell Physiology, 321(1)

ISSN

0363-6143

Authors

Manoli, Sagar S
Kisor, Kyle
Webb, Bradley A
et al.

Publication Date

2021-07-01

DOI

10.1152/ajpcell.00001.2021

Peer reviewed

Ethyl Isopropyl Amiloride Decreases Oxidative Phosphorylation and Increases Mitochondrial Fusion in Clonal Untransformed and Cancer Cells

Sagar S. Manoli[1], Kyle Kisor[1], Bradley A. Webb[2], and Diane L. Barber[1,3]

[1]Department of Cell and Tissue Biology, University of California San Francisco, San Francisco, CA

and

[2]Department of Biochemistry, West Virginia University, Morgantown, WV

Running Head: EIPA and mitochondrial function

Key words: glycolysis, intracellular pH, lactate, mitochondria, oxidative phosphorylation

Abbreviations used: EIPA, Ethyl Isopropyl Amiloride; LDHA, lactate dehydrogenase A; MCTs, monocarboxylate transporters; NHE1, Na-H exchanger isoform 1; OCR, oxygen consumption rate; pHi, intracellular (cytosolic) pH

[3]Corresponding author
Diane L. Barber
Box 0512
513 Parnassus Ave
San Francisco, CA 94143
Phone: 415-476-3764
FAX: 415-502-7338
Email: diane.barber@ucsf.edu

Abstract

Many cancer cells, regardless of their tissue origin or genetic landscape, have increased expression or activity of the plasma membrane Na-H exchanger NHE1 and a higher intracellular pH (pHi) compared with untransformed cells. A current perspective that remains to be validated is that increased NHE1 activity and pHi enable a Warburg-like metabolic reprogramming of increased glycolysis and decreased mitochondrial oxidative phosphorylation. We tested this perspective and find it is not accurate for clonal pancreatic and breast cancer cells. Using the pharmacological reagent ethyl isopropyl amiloride (EIPA) to inhibit NHE1 activity and decrease pHi, we observe no change in glycolysis, as indicated by secreted lactate and intracellular pyruvate, despite confirming increased activity of the glycolytic enzyme phosphofructokinase-1 at higher pH. Also, in contrast to predictions, we find a significant decrease in oxidative phosphorylation with EIPA, as indicated by oxygen consumption rate (OCR). Decreased OCR with EIPA is not associated with changes in pathways that fuel oxidative phosphorylation or with mitochondrial membrane potential but occurs with a change in mitochondrial dynamics that includes a significant increase in elongated mitochondrial networks, suggesting increased fusion. These findings conflict with current paradigms on increased pHi inhibiting oxidative phosphorylation and increased oxidative phosphorylation being associated with mitochondrial fusion. Moreover, these findings raise questions on the suggested use of EIPA-like compounds to limit metabolic reprogramming in cancer cells.

Introduction

Metabolic reprogramming is considered a hallmark of cancer cells that often includes increased glycolysis and decreased mitochondrial oxidative phosphorylation (24, 60) to generate biomass for fueling rapid proliferation. Although it is widely accepted that cancer cells predominantly convert glucose to lactate, either due to increased expression of the converting enzyme lactate dehydrogenase A (LDHA) (18, 66) or an impaired mitochondrial pyruvate import carrier (51), the functional status of mitochondria in cancer cells remains controversial. Cancer cells are reported to have dysfunctional mitochondria (3, 7, 46) but in contrast, the TCA cycle in mitochondria often remains a major source for ATP and functional mitochondria are essential for cancer cells to survive during tumor progression (59, 60, 67).

Another distinctive feature of most cancer cells is a constitutively higher intracellular pH (pHi) compared with untransformed cells (13, 45, 61, 64). Although initially considered a conundrum based on metabolic acids produced by rapidly proliferating cancer cells, the higher pHi of cancer cells is now known to be in-part determined by increased activity or expression of acid extruding plasma membrane ion transporters, including the Na-H exchanger, NHE1, monocarboxylate transporters (MCTs), Na+/HCO3- co-transporters, and V-ATPases (13, 45, 52, 55). The higher pHi of cancer cells is suggested to enable metabolic reprogramming and a shift from reliance on oxidative phosphorylation to glycolysis or glutaminolysis (13, 45, 61, 64); however, this has not been conclusively determined. Additionally, metabolic (26, 38, 56) and pHi (11, 36) heterogeneity occurs in cancers but whether or how these parameters might be linked

in determining their heterogeneity has received limited attention (11, 39). These considerations are important because tumor heterogeneity is a challenge for effective cancer therapies.

We addressed a number of questions on pHi dynamics and cancer cell metabolism in studies using human clonal pancreatic cancer BxPC3 cells and breast cancer MDA-MB-157 cells. We focused on these cell types because our initial studies indicated that BxPC3 but not MDA-MB-157 cells show a metabolic reprogramming of increased glycolysis and decreased oxidative phosphorylation compared with untransformed tissue-matched clonal epithelial cells, which give us models with contrasting metabolic profiles. Additionally, emerging findings indicate that features of metabolic reprogramming are different across cancer subtypes (34). We found that pharmacologically inhibiting NHE1 and lowering pHi has no effect on glycolysis but markedly decreases oxidative phosphorylation and increases mitochondrial fusion to a more tubular network. These effects are seen in both clonal cancer cells as well as in clonal untransformed pancreatic and mammary epithelial cells. Our findings challenge two current views; first, that increased activity of NHE1 and a higher pHi enable glycolysis and limit oxidative phosphorylation in cancer cells, and second, that mitochondrial fusion is associated with increased oxidative phosphorylation.

Materials and Methods

Cell lines. Clonal BxPC3 human pancreatic cancer cells obtained from Rushika Perera (UCSF) and H1299 human lung cancer cells obtained from ATCC were maintained in RPMI-1640 medium supplemented with 10% FBS, PANC-1 human pancreatic cancer cells obtained from Rushika Perera were maintained in DMEM supplemented with 10% FBS, and HPDE untransformed human

pancreatic ductal epithelial cells, also obtained from Rushika Perera, were maintained in keratinocyte medium (ThermoFisher, 37010022) supplemented with 10% FBS. MDA-MB-157 and MDA-MB-453 triple negative human breast cancer cells obtained from ATCC were maintained in Leibovitz L15 medium supplemented with 15% FBS in the absence of CO_2, and MCF10A untransformed human mammary epithelial cells obtained from Jay Debnath (UCSF) were maintained as previously described (14). Cell lines were confirmed to be mycoplasma free as tested by rtPCR (Mycoplasma Detection Kit abm #G238) and were authenticated commercially by IDEXX BioAnalytics.

Mitochondrial stress and fuel assays. Mitochondrial oxygen consumption rate (OCR) was determined using a mito-stress assay and measured with an XF24 flux analyzer (Agilent Technologies). Cells were seeded at densities optimized to obtain a linear basal OCR between 100-300 pmol/min. Effects of the selective NHE1 inhibitor 5-(N-ethyl-N-isopropyl)-amiloride (EIPA) on OCR was determined after maintaining cells in growth medium containing 10 μM EIPA for 18-20 h. Growth medium was removed and washed with non-buffered mito-stress test assay medium (DMEM basal medium supplemented where indicated with glucose, glutamine and sodium pyruvate). MDA-MB-157 cells, grown in atmospheric conditions were washed and maintained in assay medium for 2 h before measuring OCR. Basal OCR was measured, followed by measurements with the addition of a series of mito-stress compounds as indicated by Agilent Technologies specifications (https://www.agilent.com/en/support/cell-analysis/mitochondrial-respiration-xf-cell-mito-stress-test), including successively Oligomycin (1 μM), FCCP (1 μM), Rotenone (1 μM), and Antimycin (1 μM). OCR was expressed relative to the number of cells in

each well determined at the time of the assay. Cellular ATP was determined by a luminescence assay (Cayman Chemicals Detection Assay 700410) according to manufacturer's specifications.

Intracellular pH (pHi) and NHE1 activity. Steady-state pHi was measured in cells plated for 48 h in 24-well plates and loaded with the pH-sensitive dye 2',7'-bis-(2-carboxyethyl)-5-(and-6)-carboxyfluorescein (BCECF; Invitrogen) in a HCO_3-containing buffer as previously described (23). Ratios of BCECF fluorescence at Ex 490/Em530 (pH-sensitive) and Ex440/Em530 (pH-insensitive) were measured using a SpectraMax plate reader (Molecular Devices) and calibrated to pHi by treating cells at the end of each measurement in a potassium phosphate buffer containing the protonophore nigericin (10 μM) at pH 6.5 and 7.5, as previously described (23). To experimentally lower steady-state pHi, cells were incubated in growth medium containing 10 μM EIPA for 18-20 h. Loss of NHE1 activity with EIPA was confirmed by recording pHi recovery in a Hepes buffer after an NH_4Cl-induced acid load as previously described (41).

Cellular Lactate and Pyruvate measurements. Extracellular lactic acid was measured by a modification of previously described methods (63). In brief, cells were plated in 24-well plates and grown for 48 h including treatment with EIPA for the last 20 h. For each measurement in triplicate, cells were washed and incubated for 2 h in 0.5 ml FBS- and glutamine-free medium, 50 μl of medium was collected, centrifuged to remove debris, and lactic acid in the supernatant was measured using an enzyme-linked assay in a hydrazine-glycine buffer with NAD+ as a cofactor (63). Protein concentration was measured from lysed cells remaining in the wells used to collect medium and extracellular lactic acid that was expressed relative to cell total protein for each

sample. Intracellular lactate and pyruvate were measured according to manufacturer's instructions (Cayman chemicals #700510 and 700470 respectively) in cells plated in 24 well-plates. Briefly, cells were grown for 48 h as described for extracellular lactate measurements and collected after trypsinizing. Cell counts were determined then cells were washed with 1ml of PBS and collected by centrifugation. The cell pellet was treated on ice for 5 min with 0.25M of metaphosphoric acid (MPA) to deproteinate the cells. The supernatant was collected by centrifugation, neutralized with potassium carbonate, and subjected to another centrifugation. The supernatant was immediately used for assays, which were performed in 96-well black plates as indicated by assay instructions, with fluorescence signals measured at Ex530-540nm and Em 585-595nm. The determined intracellular lactate and pyruvate were represented relative to cell number.

Recombinant human phosphofructokinase-1 (PFK1) and lactate dehydrogenase A (LDHA) expression, purification and activity. Recombinant muscle PFK1 (PFKM) was expressed and purified as previously described (62, 63). The activity of recombinant PFKM was determined at 0.5 mM fructose 6-phosphate and 4 mM ATP using an auxiliary enzyme assay linking F1,6bP production to NADH oxidation as previously reported (63). MOPS and HEPES buffers were used for pH 6.8-7.6 and 7.4-8.2, respectively. Activity was determined at pH 7.4 and 7.6 in both MOPS and HEPES buffer to confirm the buffer system does not affect activity.

hLDHA cDNA with an NH_2-terminal His tag was cloned into pFastbac HTa vector containing a baculovirus specific promoter by using the Gibson Assembly method. Baculovirus was produced using the *E.coli* strain DH10Bac containing a baculovirus shuttle vector and helper plasmid that

allow the generation of bacmid according to Bac-to-Bac Baculovirus expression system (Invitrogen Life Technologies). Insect *Spodoptera frugiperda* Sf21 cells were infected with bacmid using Cellfectin II (Invitrogen) and supernatant was collected (P1) and amplified (P2), with 200 ml of P3 supernatat used for protein expression. Post 48 h infection, *Sf21* cells were collected by centrifugation, lysed in a 10 mM potassium phosphate buffer containing 0.1 % Triton-X100 at pH 7.5 and protein was purified using cobalt resin, as we previously described (63). The activity of recombinant hLDHA was determined by using 0.2 μg of purified enzyme with 0.2 mM NADH and 0.3 mM pyruvate as substrates in 100 mM potassium phosphate buffer of pH 6.8 to 7.6 by measuring the time-dependent decrease of NADH at 340 nm.

Mitochondrial membrane potential. Mitochondrial membrane potential was measured as previously described (53). In brief, cells seeded on 35 mm MatTek dishes (MatTek Corporation) and maintained for 48 h were washed and incubated with the methyl ester form of the cationic dye tetramethylrhodamine at a final concentration of 25 nM for 15 min. Unincorporated dye was removed by washing with a HEPES buffer, and basal rhodamine fluorescence intensity was acquired by spinning disk confocal imaging using an environmentally controlled inverted microscope stand (Nikon TI) equipped with a motorized TIRF illuminator (Nikon), an iXon electron-multiplying CCD camera (Andor) and a 100x 1.49 numerical aperture CFI objective (Nikon) controlled by NIS-Elements software 4.3 (Nikon). The $\Delta\psi m$ was then quenched with FCCP (10 μM) and then images were again acquired using identical field of views as controls. Data were expressed as the ratio of basal/FCCP fluorescent intensity, with image processing and analysis performed using NIS-Elements software.

Immunobloting for AMPK and measurement of cellular ATP. Proteins in 20-30 μg of total cell lysate were separated by 10% SDS, transferred to Imobilon membranes and immunoblotted as previously described (65). Membranes were probed with antibodies to phosphorylated AMPK and total AMPK (1:1000; Cell Signaling Technology #2535 and #2532, respectively). Cellular ATP was determined using a luminescence assay according to manufacturer's instructions (Cayman #700410) and cells plated in 24 well-plates. Data were normalized to cell number determined in parallel samples and expressed as cellular ATP with EIPA relative to control.

Mitochondrial morphology. For imaging, mitochondria were stained using Mitotracker DeepRed™ (Life Technologies #D12345) according to the manufacturer specifications. In brief, cells were seeded at ~25% confluence in 35 mm glass bottom MatTek dishes, maintained for 24 h in growth medium, and then live cells were stained with 25 nM Mitotracker DeepRed™ for 15 min. Excess stain was washed and Z-stack images of 0.1 μm were obtained with a 100x objective and spinning disk confocal microscope as described for $\Delta\psi m$. Reconstructions of images were generated and mitochondrial length quantified by using Imaris image analysis software with surface function and default thresholding settings.

Data presentation and statistical analysis. Box-and whisker plots were generated using Analyse-It for Microsoft Excel and show median, first and third quartile, observations within 1.5 times the interquartile range, and all individual data points. Significance of multiple comparisons was calculated by Tukey–Kramer honest significant difference (HSD) test in Analyse-It for Microsoft.

Bar graphs were generated using Excel or Prism software with significance determined using Student's Paired *t*-test. Figures were assembled in Adobe Illustrator CS5.

Results

EIPA decreases basal and maximal respiratory capacity of cells.

In cancer cells, increased NHE1 activity is predicted to enable metabolic reprogramming by increasing glycolysis and suppressing mitochondrial oxidative phosphorylation (13, 45, 61, 64). To our knowledge, however, this prediction has not been experimentally verified. To address this prediction, we tested a series of clonal cancer cells and chose to focus further on BxPC3 human pancreatic ductal adenocarcinoma cells and MDA-MB-157 human triple-negative breast cancer cells. Our criteria for selecting these cells included published data on differences in metabolic profiles of clonal cancer cells, using cancer cells with established tissue-matched untransformed cells (HPDE for BxPC3 and MCF10A for MDA-MB-157) and our data on pHi in the absence and presence of EIPA (Supplementary Fig. S1A). For example, although BxPC3 and PANC-1 pancreatic ductal adenocarcinoma cells have distinct metabolic profiles (37) and a higher pHi than untransformed HPDE cells (Fig. S1A), EIPA significantly decreased pHi in BxPC3 cells but not PANC-1 cells. Additionally, EIPA had no effect on pHi of MDA-MB-453 human breast cancer cells or H1299 human lung cancer cells (Supplementary Fig. S1A); hence we did not include these cells for further study.

BxPC3 but not MDA-MB-157 cells showed decreased oxidative phosphorylation compared with tissue-matched untransformed epithelial cells (Fig. 1A and E). We determined oxidative phosphorylation by measuring oxygen consumption rate (OCR) in growing cells using

the well-established mitochondrial stress test and a Seahorse XF Analyzer (17). After measuring basal OCR, a series of mitochondrial membrane transport inhibitors were injected, including Oligomycin (1 μM) to determine ATP-linked respiration, FCCP (1 μM) to determine maximal respiration, and Antimycin (1 μM) + Rotenone (1 μM) to determine spare respiratory capacity (Fig. 1A). We used the mitochondrial stress test with untreated control cells and with cells treated with EIPA (10 μM) for 18-20 h to selectively inhibit activity of NHE1, a H+ extruder. We confirmed treatment with EIPA completely inhibited NHE1 activity in BxPC3 and MDA-MB-157 cells, determined by loss of pHi recovery from an acid load (Supplementary Fig. S1B, C), and decreased pHi in all cells used in our study (Supplementary Fig. S1A). Our pHi measurements indicate that control pHi in BxPC3 and MDA-MB-157 cells was significantly higher than tissue-matched non-transformed cells and also that NHE1 activity contributes substantially to steady-state pHi in these cells. We chose to pharmacologically inhibit NHE1 activity rather than genetically silence NHE1 because the exchanger has functions in addition to ion transport, including its C-terminal cytoplasmic domain functioning as a scaffold by binding signaling proteins and anchoring actin filaments to the plasma membrane (6, 40). Additionally, long-term loss of NHE1 activity is synthetic lethal with activated oncogenes (22).

We found that BxPC3 cells had a lower OCR compared with untransformed HPDE human normal pancreatic ductal epithelial cells (Fig. 1A), including basal OCR (Fig. 1C) and maximal respiration (Fig 1D). Although OCR with BxPC3 cells is reported to be markedly lower compared with a number of other pancreatic ductal adenocarcinoma cells, including PANC-1 and Mia-PaCa2 (37); this report did not include OCR for untransformed human pancreatic ductal epithelial cells. In contrast to the prediction described above of increased NHE1 activity suppressing oxidative

phosphorylation, we found that EIPA decreased OCR in both BxPC3 and HPDE cells, with significantly decreased basal OCR (Fig. 1C) and maximal respiration (Fig 1D).

In contrast to BxPC3 and HPDE cells, the OCR for MDA-MB-157 breast cancer cells and untransformed MCF10A human mammary epithelial cells was not different (Fig. 1E), including no difference in basal OCR (Fig. 1G) and maximal respiration (Fig 1H). However, in both cell types, EIPA decreased OCR, including basal OCR and maximal respiration (Fig. 1F-H). These data indicate that BxPC3 cells have a higher pHi and lower OCR than HPDE cells, and that MDA-MB-157 also have a higher pHi but not different basal OCR or maximal respiration compared with MCF10A cells. However, in contrast to the prediction that increased NHE1 activity and pHi suppress oxidative phosphorylation, inhibiting NHE1 activity with EIPA decreased OCR in all four cell types.

EIPA does not change glycolysis despite pH-regulated activity of phosphofructokinase-1

Consistent with BxPC3 cells showing metabolic reprograming with decreased oxidative phosphorylation, these cells also had increased secreted lactate compared with untransformed HPDE cells (Fig. 2A), suggesting increased glycolysis. For MDA-MB-157 cells, although OCR is not different compared with untransformed MCF10A cells, secreted lactate is significantly less (Fig. 2B), suggesting a lower glycolytic rate. However, despite EIPA decreasing OCR in all of these cells, it had no effect on amounts of secreted lactate (Fig. A, B). We also measured intracellular lactic acid in MDA-MB-157 cells, which was not different in the absence compared with the presence of EIPA (Supplementary Fig. 2A).

To further test glycolysis we measured intracellular pyruvate, a metabolite upstream of lactate, which was significantly lower in BXPC3 compared to HPDE cells (Fig. 2C), suggesting

BxPC3 cells may be more effectively converting pyruvate to lactate. Additionally, despite MCF10A cells having more secreted lactic acid than MDA-MB-157 cells, levels of intracellular pyruvate were not different in these two cell types (Fig. 2C). However, in all four cell types EIPA has no effect on secreted lactate or intracellular pyruvate, which strongly suggests it does not alter glycolytic flux.

The prediction that increased NHE1 activity and pHi in cancer cells increases glycolysis to enable metabolic reprogramming is in part based on previous work showing that activity of phosphofructokinase-1 (PFK1), which catalyzes the rate-limiting step committing glucose to breakdown, is pH sensitive with increased activity at higher pH (16, 58). Additionally, lactate dehydrogenase A (LDHA), an enzyme catalyzing the conversion of pyruvate to lactate is reported to be pH sensitive, with yeast LDH having increased activity at higher pH (20, 54) and the M but not H isoform of recombinant human muscle LDH having increased activity with increasing pH above 7.0 (47). In contrast, recombinant human LDH was recently found to have promiscuous reduction of alpha-keto-glutarate to 2-hydroxyglutarate at acidic pH (29, 43).

To further reconcile our findings on glycolysis with reported effects of pH on activity of PFK1 and LDHA, we generated and purified recombinant human enzymes (Supplementary Fig. 2B, C) and determined the effect of pH on activity of the enzymes. Although all three PFK1 isoforms, muscle, platelet and liver, have increased activity at higher pH (1, 48, 58), the muscle isoform, PFKM, is most sensitive to pH and has pH-dependent relief of allosteric inhibition by ATP. Using recombinant human PFKM generated in a baculovirus expression system to enable post-translational modifications that might affect activity, we found that PFKM activity was pH-dependent with increased activity at high pH (Fig. 2D). The data indicated a distinct linear

increase in activity from ~ 7.2 to ~ 7.7, which is very consistent with findings using purified native PFKM (16, 58). In contrast, activity of recombinant purified human LDHA, also generated using a baculovirus expression system, was not different within the range of pH 6.8 to 7.5 (Fig. 2E). Our finding of increased PFKM with higher pHi does coincide with no change in glycolysis when pHi is decreased with EIPA. However, we cannot not rule out possible effects of pHi on PFK1 activity in cells that could be mediated by other isoforms, changes in substrate or the activity of other glycolytic enzymes.

EIPA does not change fatty acid, glutamine- or pyruvate-fueled OCR and has no effect on mitochondrial membrane potential

Mitochondrial respiration is regulated by metabolites from fatty acid oxidation (FAO), glutaminolysis, and glycolysis. To determine how EIPA might decrease basal OCR we tested whether it limits how these pathways fuel mitochondrial respiration. We quantified the contribution of each pathway by measuring basal OCR in the absence and presence of selective inhibitors of each pathway, including Etomoxir for FAO, BPTES for glutaminolysis and UK5099 for the mitochondrial pyruvate carrier. We focused on HPDE and BxPC3 cells because in control conditions they had distinct OCR values but MCF10 and MDA-MB-157 cells did not (Fig. 1A, E). In addition to HPDE and BxPC3 cells having different basal and maximal respiration, they also had differences in the pathways that fuel OCR. We found that dependence on FAO was ~ 9% in HPDE cells but ~ 40% for BxPC3 cells, dependence on glutaminolysis was nearly undetectable in HPDE cells but ~ 16% in BxPC3 cells, and dependence on pyruvate was ~ 4% in HPDE cells but ~ 14% in BxPC3 cells (Fig. 3A). The significantly higher contributions from FAO and glutaminolysis in BxPC3 cells compared with HPDE cells is consistent with upregulated FAO in many cancer types (34) and

pancreatic cancers being reliant on glutaminolysis pathways (8). However, although EIPA lowered basal OCR in HPDE and BxPC3 cells, it had no effect on the relative contribution of FAO (Supplementary Fig. 3A), glutaminolysis, or pyruvate (data not shown) we observe in control cells. Oxidative phosphorylation is also regulated by phosphorylated AMP kinase (pAMPK), an indicator of cellular ATP levels and bioenergetics, and by mitochondrial membrane potential ($\Delta\psi m$). Although EIPA decreased ATP-linked OCR, determined as basal OCR minus OCR with Oligomycin (Supplementary Fig. 3B), it had no effect on pAMPK in BxPC3 cells, determined by immunoblotting (Supplementary Fig. 3C) or cellular ATP concentration in the four cell lines we studied (Supplementary Fig. 3D). EIPA also had no effect on $\Delta\psi m$, determined by quantifying confocal images of BxPC3 cells loaded with the methyl ester of the cationic dye tetramethylrhodamine (Fig. 3B, C). Hence, although inhibiting NHE1 activity with EIPA decreased basal and maximal OCR in BxPC3 cells, it had no marked effect on the contribution of pathways fueling OCR or bioenergetics level as indicated by pAMPK, cellular ATP or $\Delta\psi m$.

EIPA induces tubular mitochondrial structure.

Yet another regulator of OCR is mitochondrial morphology, which we found is markedly changed with EIPA. Changes in mitochondrial morphology, termed mitochondrial dynamics, includes the processes of fission, or the division or fragmentation of individual mitochondrion, and fusion, or the union of mitochondria generally into a tubular network. We used images of live cells stained with Mitotracker DeepRed^{TM} and imaged by spinning disk confocal microscopy to generate reconstructions of mitochondrial morphology (Fig. 4A) and to quantify mitochondrial lengths with Imaris software (Fig. 4B-E). We binned mitochondrial lengths into four categories,

0-5 µm, 5-20 µm, 20-50 µm and > 50 µm, and expressed data as a percent of mitochondria within each length range. Quantification indicated that mitochondria morphology of control cells was predominantly in the intermediate range of 5 to 50 µm, with BxPC3 having substantially fewer mitochondria of > 50 µm, With EIPA, however, all four cell types had significantly fewer mitochondria of 5-20 µm length and more > 50 µm, indicating an increased tubular network (Fig. 4C-F). Visually, control cells appear to have a more compact mitochondrial network, and with EIPA cells are more spread with a less compact network (Fig. 4A). This observation was most pronounced for MDA-MBA-157 cells, despite OCR not being different in MDA-MB-157 and MCF10A cells. A current view is that elongated mitochondrial networks are associated with increased oxidative phosphorylation (42). However, our findings indicate that EIPA changes mitochondrial dynamics to a more elongated tubular network, suggesting increased fusion, despite EIPA decreasing OCR.

Supplementary data can be found at https://doi.org/10.6084/m9.figshare.14633286

Discussion

Our study tests a commonly conveyed prediction that in cancer cells increased activity of NHE1 and a higher pHi enable metabolic reprogramming by suppressing mitochondrial oxidative phosphorylation and increasing glycolysis (45, 61, 64). Contrary to this prediction, however, we found that inhibiting NHE1 activity and decreasing pHi with EIPA decreased oxidative phosphorylation in clonal cancer and untransformed cells, determined by measuring oxygen consumption rates, and had no effect on glycolysis, determined by measuring extracellular lactate and intracellular pyruvate. In HEK cells, the NHE1 inhibitor cariporide also has no effect

on steady-state lactate production (50) and to our knowledge the MCT lactate-H+ transporters are not sensitive to EIPA . We confirmed that recombinant PFKM generated to include post-translational modifications has increased activity at higher pH, as previously reported for native enzyme isolated from muscle (16, 58). The lack of an effect of decreased pHi on glycolysis despite pH dependent PFKM activity could reflect the relative expression of muscle compared platelet and liver isoforms. However, the activity of these isoforms also is greater at higher pH, albeit with less sensitivity than PFKM (1, 48, 58). We found no effect of pH within the physiological range on activity of purified recombinant LDHA, despite conflicting findings that yeast (20, 54) and human (47) LDH have increased activity at higher pH and that recombinant mammalian LDH has promiscuous increased activity at more acidic pH (29, 43). Moreover, our findings contrast to an NHE1-dependent increase in glycolysis induced by human carcinogens (25).

Although EIPA decreased oxygen consumption rate in cancer and untransformed cells, it had no effect on contributions of distinct metabolic pathways to mitochondrial respiration, including FAO, glutaminolysis, and glycolysis, or on mitochondrial membrane potential. However, EIPA did induce marked changes in mitochondrial morphology, increasing mitochondria lengths and a more tubular network in the cancer as well as non-transformed cells we studied. Our findings are in contrast to a current view that elongated mitochondrial networks are associated with increased oxidative phosphorylation (42). However, extracellular acidosis, a feature of tumors like increased pHi, promotes mitochondria fusion and limits fragmentation (33). Moreover, Nehrke and colleagues report links between a Na-H exchanger, pHi, and mitochondrial morphology in *C. elegans*, with chronic mitochondrial fragmentation lowering pHi (31) and in *C.*

elegans and mammalian cells a lower pHi inhibits mitochondrial fusion with effects mediated by reactive oxygen species (ROS) (30). Although increased ROS inhibits NHE1 expression and/or activity and lowers pHi (2, 44), whether EIPA regulates ROS abundance remains unclear. EIPA inhibits increases in ROS (4, 12), which can be mediated by decreased NHE1 activity. In contrast, however, cell injury stress is recently reported to increase redox signaling and mitochondrial fission (28), although this study does not include effects on mitochondrial respiration. Hence, there remains caution on an oversimplified assumption that mitochondrial fusion is associated with increased oxidative phosphorylation, and as suggested, correlations between mitochondrial dynamics and metabolism remain unclear (9).

Our experimental design does not rule out a direct effect of EIPA on mitochondrial morphology; although if this occurs it is not likely mediated by a Na-H exchanger. A mitochondrial localized NHE isoform distinct from plasma membrane NHE1 remains controversial. A mitochondrial cation/proton exchange by NHA2 (SLC9B2) is reported (5, 19); however, in isolated mitochondria EIPA has no effect on H+ transport (32) or respiration (15) at concentrations up to 100 μM, compared with the 10 μM we used in our study. A recent study shows that long-term (5 days) but not short-term (1 day) treatment with EIPA has cytotoxic effects independent of NHE1 (49).

In addition to possible bi-directional effects of EIPA on oxidative phosphorylation and mitochondrial morphology, the decreased OCR we observed with EIPA could reflect decreased micropinocytosis because this cellular uptake process is inhibited by amiloride (35) and EIPA (10), with effects of EIPA shown using BxPC3 cells as we used in our study. An additional and not mutually exclusive mechanism mediating decreased OCR with EIPA could be effects on

intracellular Ca^{2+}, which is lowered by EIPA (21, 57), although possibly secondary to lowering pHi. Additionally, decreasing Ca^{2+} entry by the Trpm2 channel decreases OCR (27).

Further studies are needed to resolve effects of EIPA on mitochondrial respiration and morphology and whether they are mediated by decreased NHE1 activity and lower pHi. Our findings that a lower pHi is associated with decreased OCR raise questions on the prevailing prediction that the higher pHi of cancer cells enables metabolic reprogramming by suppressing oxidative phosphorylation and also for lowering pHi as a therapeutic strategy to limit cancer progression by reversing metabolic reprogramming

Acknowledgements

We thank Rushika Perera for providing BxPC3 and HPDE cells and Jay Debnath for providing MCF10A cells. Seahorse Instrumentation was available through the UCSF Mouse Metabolism Core within the Nutrition Obesity Center that is supported by National Institutes of Health grant 1P30DK098722. This work was supported by National Institutes of Health grants CA937855 to DLB and CA197855-04S1 to KK.

Disclosure

The authors disclose no perceived or potential conflict of interest, financial or otherwise.

References

1. **Akkerman JW, Gorter G, Sixma JJ, and Staal GE**. Human platelet 6-phosphofructokinase. Purification, kinetic parameters and the influence of sulphate ions on enzyme activity. *Biochim Biophys Acta* 370: 102-112, 1974.
2. **Akram S, Teong HF, Fliegel L, Pervaiz S, and Clement MV**. Reactive oxygen species-mediated regulation of the Na+-H+ exchanger 1 gene expression connects intracellular redox status with cells' sensitivity to death triggers. *Cell Death Differ* 13: 628-641, 2006.
3. **Arora R, Schmitt D, Karanam B, Tan M, Yates C, and Dean-Colomb W**. Inhibition of the Warburg effect with a natural compound reveals a novel measurement for determining the metastatic potential of breast cancers. *Oncotarget* 6: 662-678, 2015.
4. **Baldini PM, De Vito P, Martino A, Fraziano M, Grimaldi C, Luly P, Zalfa F, and Colizzi V**. Differential sensitivity of human monocytes and macrophages to ANP: a role of intracellular pH on reactive oxygen species production through the phospholipase involvement. *J Leukoc Biol* 73: 502-510, 2003.
5. **Battaglino RA, Pham L, Morse LR, Vokes M, Sharma A, Odgren PR, Yang M, Sasaki H, and Stashenko P**. NHA-oc/NHA2: a mitochondrial cation-proton antiporter selectively expressed in osteoclasts. *Bone* 42: 180-192, 2008.
6. **Baumgartner M, Patel H, and Barber DL**. Na(+)/H(+) exchanger NHE1 as plasma membrane scaffold in the assembly of signaling complexes. *Am J Physiol Cell Physiol* 287: C844-850, 2004.
7. **Boland ML, Chourasia AH, and Macleod KF**. Mitochondrial dysfunction in cancer. *Front Oncol* 3: 292, 2013.
8. **Bott AJ, Shen J, Tonelli C, Zhan L, Sivaram N, Jiang YP, Yu X, Bhatt V, Chiles E, Zhong H, Maimouni S, Dai W, Velasquez S, Pan JA, Muthalagu N, Morton J, Anthony TG, Feng H, Lamers WH, Murphy DJ, Guo JY, Jin J, Crawford HC, Zhang L, White E, Lin RZ, Su X, Tuveson DA, and Zong WX**. Glutamine Anabolism Plays a Critical Role in Pancreatic Cancer by Coupling Carbon and Nitrogen Metabolism. *Cell Rep* 29: 1287-1298 e1286, 2019.
9. **Chen H, and Chan DC**. Mitochondrial Dynamics in Regulating the Unique Phenotypes of Cancer and Stem Cells. *Cell Metab* 26: 39-48, 2017.
10. **Commisso C, Davidson SM, Soydaner-Azeloglu RG, Parker SJ, Kamphorst JJ, Hackett S, Grabocka E, Nofal M, Drebin JA, Thompson CB, Rabinowitz JD, Metallo CM, Vander Heiden MG, and Bar-Sagi D**. Macropinocytosis of protein is an amino acid supply route in Ras-transformed cells. *Nature* 497: 633-637, 2013.
11. **Corbet C, and Feron O**. Tumour acidosis: from the passenger to the driver's seat. *Nat Rev Cancer* 17: 577-593, 2017.
12. **Dailianis S, Piperakis SM, and Kaloyianni M**. Cadmium effects on ros production and DNA damage via adrenergic receptors stimulation: role of Na+/H+ exchanger and PKC. *Free Radic Res* 39: 1059-1070, 2005.
13. **Damaghi M, Wojtkowiak JW, and Gillies RJ**. pH sensing and regulation in cancer. *Front Physiol* 4: 370, 2013.
14. **Debnath J, Muthuswamy SK, and Brugge JS**. Morphogenesis and oncogenesis of MCF-10A mammary epithelial acini grown in three-dimensional basement membrane cultures. *Methods* 30: 256-268, 2003.

15. **Dlaskova A, Hlavata L, Jezek J, and Jezek P**. Mitochondrial Complex I superoxide production is attenuated by uncoupling. *Int J Biochem Cell Biol* 40: 2098-2109, 2008.
16. **Dobson GP, Yamamoto E, and Hochachka PW**. Phosphofructokinase control in muscle: nature and reversal of pH-dependent ATP inhibition. *Am J Physiol* 250: R71-76, 1986.
17. **Eriksson M, Ambroise G, Ouchida AT, Lima Queiroz A, Smith D, Gimenez-Cassina A, Iwanicki MP, Muller PA, Norberg E, and Vakifahmetoglu-Norberg H**. Effect of Mutant p53 Proteins on Glycolysis and Mitochondrial Metabolism. *Mol Cell Biol* 37: 2017.
18. **Fantin VR, St-Pierre J, and Leder P**. Attenuation of LDH-A expression uncovers a link between glycolysis, mitochondrial physiology, and tumor maintenance. *Cancer Cell* 9: 425-434, 2006.
19. **Fuster DG, Zhang J, Shi M, Bobulescu IA, Andersson S, and Moe OW**. Characterization of the sodium/hydrogen exchanger NHA2. *J Am Soc Nephrol* 19: 1547-1556, 2008.
20. **Gaspar P, Neves AR, Shearman CA, Gasson MJ, Baptista AM, Turner DL, Soares CM, and Santos H**. The lactate dehydrogenases encoded by the ldh and ldhB genes in Lactococcus lactis exhibit distinct regulation and catalytic properties - comparative modeling to probe the molecular basis. *FEBS J* 274: 5924-5936, 2007.
21. **Goldman A, Chen H, Khan MR, Roesly H, Hill KA, Shahidullah M, Mandal A, Delamere NA, and Dvorak K**. The Na+/H+ exchanger controls deoxycholic acid-induced apoptosis by a H+-activated, Na+-dependent ionic shift in esophageal cells. *PLoS One* 6: e23835, 2011.
22. **Grillo-Hill BK, Choi C, Jimenez-Vidal M, and Barber DL**. Increased H(+) efflux is sufficient to induce dysplasia and necessary for viability with oncogene expression. *Elife* 4: 2015.
23. **Grillo-Hill BK, Webb BA, and Barber DL**. Ratiometric imaging of pH probes. *Methods Cell Biol* 123: 429-448, 2014.
24. **Hanahan D, and Weinberg RA**. Hallmarks of cancer: the next generation. *Cell* 144: 646-674, 2011.
25. **Hardonniere K, Huc L, Sergent O, Holme JA, and Lagadic-Gossmann D**. Environmental carcinogenesis and pH homeostasis: Not only a matter of dysregulated metabolism. *Semin Cancer Biol* 43: 49-65, 2017.
26. **Hensley CT, Faubert B, Yuan Q, Lev-Cohain N, Jin E, Kim J, Jiang L, Ko B, Skelton R, Loudat L, Wodzak M, Klimko C, McMillan E, Butt Y, Ni M, Oliver D, Torrealba J, Malloy CR, Kernstine K, Lenkinski RE, and DeBerardinis RJ**. Metabolic Heterogeneity in Human Lung Tumors. *Cell* 164: 681-694, 2016.
27. **Hoffman NE, Miller BA, Wang J, Elrod JW, Rajan S, Gao E, Song J, Zhang XQ, Hirschler-Laszkiewicz I, Shanmughapriya S, Koch WJ, Feldman AM, Madesh M, and Cheung JY**. Ca(2)(+) entry via Trpm2 is essential for cardiac myocyte bioenergetics maintenance. *Am J Physiol Heart Circ Physiol* 308: H637-650, 2015.
28. **Horn A, Raavicharla S, Shah S, Cox D, and Jaiswal JK**. Mitochondrial fragmentation enables localized signaling required for cell repair. *J Cell Biol* 219: 2020.
29. **Intlekofer AM, Wang B, Liu H, Shah H, Carmona-Fontaine C, Rustenburg AS, Salah S, Gunner MR, Chodera JD, Cross JR, and Thompson CB**. L-2-Hydroxyglutarate production arises from noncanonical enzyme function at acidic pH. *Nat Chem Biol* 13: 494-500, 2017.
30. **Johnson D, Allman E, and Nehrke K**. Regulation of acid-base transporters by reactive oxygen species following mitochondrial fragmentation. *Am J Physiol Cell Physiol* 302: C1045-1054, 2012.

31. **Johnson D, and Nehrke K**. Mitochondrial fragmentation leads to intracellular acidification in Caenorhabditis elegans and mammalian cells. *Mol Biol Cell* 21: 2191-2201, 2010.
32. **Kapus A, Lukacs GL, Cragoe EJ, Jr., Ligeti E, and Fonyo A**. Characterization of the mitochondrial Na+-H+ exchange. The effect of amiloride analogues. *Biochim Biophys Acta* 944: 383-390, 1988.
33. **Khacho M, Tarabay M, Patten D, Khacho P, MacLaurin JG, Guadagno J, Bergeron R, Cregan SP, Harper ME, Park DS, and Slack RS**. Acidosis overrides oxygen deprivation to maintain mitochondrial function and cell survival. *Nat Commun* 5: 3550, 2014.
34. **Kim J, and DeBerardinis RJ**. Mechanisms and Implications of Metabolic Heterogeneity in Cancer. *Cell Metab* 30: 434-446, 2019.
35. **Koivusalo M, Welch C, Hayashi H, Scott CC, Kim M, Alexander T, Touret N, Hahn KM, and Grinstein S**. Amiloride inhibits macropinocytosis by lowering submembranous pH and preventing Rac1 and Cdc42 signaling. *J Cell Biol* 188: 547-563, 2010.
36. **Korenchan DE, and Flavell RR**. Spatiotemporal pH Heterogeneity as a Promoter of Cancer Progression and Therapeutic Resistance. *Cancers (Basel)* 11: 2019.
37. **Kovalenko I, Glasauer A, Schockel L, Sauter DR, Ehrmann A, Sohler F, Hagebarth A, Novak I, and Christian S**. Identification of KCa3.1 Channel as a Novel Regulator of Oxidative Phosphorylation in a Subset of Pancreatic Carcinoma Cell Lines. *PLoS One* 11: e0160658, 2016.
38. **Lanning NJ, Castle JP, Singh SJ, Leon AN, Tovar EA, Sanghera A, MacKeigan JP, Filipp FV, and Graveel CR**. Metabolic profiling of triple-negative breast cancer cells reveals metabolic vulnerabilities. *Cancer Metab* 5: 6, 2017.
39. **Lobo RC, Hubbard NE, Damonte P, Mori H, Penzvalto Z, Pham C, Koehne AL, Go AC, Anderson SE, Cala PM, and Borowsky AD**. Glucose Uptake and Intracellular pH in a Mouse Model of Ductal Carcinoma In situ (DCIS) Suggests Metabolic Heterogeneity. *Front Cell Dev Biol* 4: 93, 2016.
40. **Meima ME, Mackley JR, and Barber DL**. Beyond ion translocation: structural functions of the sodium-hydrogen exchanger isoform-1. *Curr Opin Nephrol Hypertens* 16: 365-372, 2007.
41. **Meima ME, Webb BA, Witkowska HE, and Barber DL**. The sodium-hydrogen exchanger NHE1 is an Akt substrate necessary for actin filament reorganization by growth factors. *J Biol Chem* 284: 26666-26675, 2009.
42. **Mishra P, and Chan DC**. Metabolic regulation of mitochondrial dynamics. *J Cell Biol* 212: 379-387, 2016.
43. **Nadtochiy SM, Schafer X, Fu D, Nehrke K, Munger J, and Brookes PS**. Acidic pH Is a Metabolic Switch for 2-Hydroxyglutarate Generation and Signaling. *J Biol Chem* 291: 20188-20197, 2016.
44. **Nakamura U, Iwase M, Uchizono Y, Sonoki K, Sasaki N, Imoto H, Goto D, and Iida M**. Rapid intracellular acidification and cell death by H2O2 and alloxan in pancreatic beta cells. *Free Radic Biol Med* 40: 2047-2055, 2006.
45. **Parks SK, Chiche J, and Pouyssegur J**. Disrupting proton dynamics and energy metabolism for cancer therapy. *Nat Rev Cancer* 13: 611-623, 2013.

46. **Pelicano H, Zhang W, Liu J, Hammoudi N, Dai J, Xu RH, Pusztai L, and Huang P**. Mitochondrial dysfunction in some triple-negative breast cancer cell lines: role of mTOR pathway and therapeutic potential. *Breast Cancer Res* 16: 434, 2014.
47. **Read JA, Winter VJ, Eszes CM, Sessions RB, and Brady RL**. Structural basis for altered activity of M- and H-isozyme forms of human lactate dehydrogenase. *Proteins* 43: 175-185, 2001.
48. **Reinhart GD**. Influence of pH on the regulatory kinetics of rat liver phosphofructokinase: a thermodynamic linked-function analysis. *Biochemistry* 24: 7166-7172, 1985.
49. **Rolver MG, Elingaard-Larsen LO, Andersen AP, Counillon L, and Pedersen SF**. Pyrazine ring-based Na(+)/H(+) exchanger (NHE) inhibitors potently inhibit cancer cell growth in 3D culture, independent of NHE1. *Sci Rep* 10: 5800, 2020.
50. **Rotte A, Pasham V, Eichenmuller M, Bhandaru M, Foller M, and Lang F**. Upregulation of Na+/H+ exchanger by the AMP-activated protein kinase. *Biochem Biophys Res Commun* 398: 677-682, 2010.
51. **Schell JC, Olson KA, Jiang L, Hawkins AJ, Van Vranken JG, Xie J, Egnatchik RA, Earl EG, DeBerardinis RJ, and Rutter J**. A role for the mitochondrial pyruvate carrier as a repressor of the Warburg effect and colon cancer cell growth. *Mol Cell* 56: 400-413, 2014.
52. **Stock C, and Pedersen SF**. Roles of pH and the Na(+)/H(+) exchanger NHE1 in cancer: From cell biology and animal models to an emerging translational perspective? *Semin Cancer Biol* 43: 5-16, 2017.
53. **Sukumar M, Liu J, Mehta GU, Patel SJ, Roychoudhuri R, Crompton JG, Klebanoff CA, Ji Y, Li P, Yu Z, Whitehill GD, Clever D, Eil RL, Palmer DC, Mitra S, Rao M, Keyvanfar K, Schrump DS, Wang E, Marincola FM, Gattinoni L, Leonard WJ, Muranski P, Finkel T, and Restifo NP**. Mitochondrial Membrane Potential Identifies Cells with Enhanced Stemness for Cellular Therapy. *Cell Metab* 23: 63-76, 2016.
54. **Suzuki H, and Ogura Y**. Effect of pH on the kinetic parameters of yeast L(plus)-lactate dehydrogenase (cytochrome b2). *J Biochem* 67: 291-295, 1970.
55. **Swietach P, Vaughan-Jones RD, Harris AL, and Hulikova A**. The chemistry, physiology and pathology of pH in cancer. *Philos Trans R Soc Lond B Biol Sci* 369: 20130099, 2014.
56. **Tasdogan A, Faubert B, Ramesh V, Ubellacker JM, Shen B, Solmonson A, Murphy MM, Gu Z, Gu W, Martin M, Kasitinon SY, Vandergriff T, Mathews TP, Zhao Z, Schadendorf D, DeBerardinis RJ, and Morrison SJ**. Metabolic heterogeneity confers differences in melanoma metastatic potential. *Nature* 577: 115-120, 2020.
57. **Thibonnier M, Bayer AL, Simonson MS, and Douglas JG**. Effects of amiloride analogues on AVP binding and activation of V1-receptor-expressing cells. *Am J Physiol* 262: E76-86, 1992.
58. **Trivedi B, and Danforth WH**. Effect of pH on the kinetics of frog muscle phosphofructokinase. *J Biol Chem* 241: 4110-4112, 1966.
59. **Wallace DC**. Mitochondria and cancer. *Nat Rev Cancer* 12: 685-698, 2012.
60. **Ward PS, and Thompson CB**. Metabolic reprogramming: a cancer hallmark even warburg did not anticipate. *Cancer Cell* 21: 297-308, 2012.
61. **Webb BA, Chimenti M, Jacobson MP, and Barber DL**. Dysregulated pH: a perfect storm for cancer progression. *Nat Rev Cancer* 11: 671-677, 2011.

62. **Webb BA, Dosey AM, Wittmann T, Kollman JM, and Barber DL**. The glycolytic enzyme phosphofructokinase-1 assembles into filaments. *J Cell Biol* 216: 2305-2313, 2017.
63. **Webb BA, Forouhar F, Szu FE, Seetharaman J, Tong L, and Barber DL**. Structures of human phosphofructokinase-1 and atomic basis of cancer-associated mutations. *Nature* 523: 111-114, 2015.
64. **White KA, Grillo-Hill BK, and Barber DL**. Cancer cell behaviors mediated by dysregulated pH dynamics at a glance. *J Cell Sci* 130: 663-669, 2017.
65. **White KA, Grillo-Hill BK, Esquivel M, Peralta J, Bui VN, Chire I, and Barber DL**. beta-Catenin is a pH sensor with decreased stability at higher intracellular pH. *J Cell Biol* 217: 3965-3976, 2018.
66. **Xiao X, Huang X, Ye F, Chen B, Song C, Wen J, Zhang Z, Zheng G, Tang H, and Xie X**. The miR-34a-LDHA axis regulates glucose metabolism and tumor growth in breast cancer. *Sci Rep* 6: 21735, 2016.
67. **Yang C, Ko B, Hensley CT, Jiang L, Wasti AT, Kim J, Sudderth J, Calvaruso MA, Lumata L, Mitsche M, Rutter J, Merritt ME, and DeBerardinis RJ**. Glutamine oxidation maintains the TCA cycle and cell survival during impaired mitochondrial pyruvate transport. *Mol Cell* 56: 414-424, 2014.

Figure Legends

Fig. 1. Oxygen consumption rates (OCR) for the indicated cell types and conditions. A, B. Mitochondrial stress test with HPDE and BxPC3 cells for control (A) and with EIPA (10 μM) (B). As labeled in (A), shown is basal OCR before sequentially adding mitochondrial transporter inhibitors at 1 μM, including Oligomycin for ATP-linked respiration, FCCP for maximal respiration, and Antimycin + Rotenone for spare respiratory capacity. Data are means ± s.e.m. of five separate cell preparations. C, D. Basal (C) and maximal (C) OCR for HPDE and BxPC3 cells in the absence (control) and presence of EIPA. Data are from five separate cell preparations. Box plots show median, first and third quartile, with whiskers extending to observations within 1.5 times the interquartile range, and all individual data points. Statistical analysis by Tukey-Kramer HSD test. E, F. Mitochondrial stress test as in (A) with MCF10A and MDA-MB-157 cells for control (E) and with EIPA (F). Data are means ± s.e.m. of five separate cell preparations. G, H. Basal (C) and maximal (C) OCR for HPDE and BxPC3 cells in the absence (control) and presence of EIPA. Data are from five separate cell preparations with Box plots and statistical analysis as described for C and D.

Fig. 2. Glycolysis and activity of the glycolytic enzymes PFK1 and LDHA. A, B. Lactic acid secreted from HPDE and BxPC3 cells (A) and MCF10A and MDA-MB-157 cells (B) in the absence (control) and presence of EIPA (10 μM). Data are from four (A) and three (B) separate cell preparations. Box plots show median, first and third quartile, with whiskers extending to observations within 1.5 times the interquartile range, and all individual data points. Statistical analysis by Tukey-Kramer HSD test. C. Intracellular pyruvate for the indicated cell types and conditions. Data are

means ± s.e.m. of three separate cell preparations, with statistical analysis using Student's Paired *t*-test D. Activity of PFKM, expressed relative to maximal activity at 4 mM ATP and 0.5 mM fructose 6-phosphate. Data are means ± s.e.m. of seven separate measurements with two different protein preparations. E. Activity, expressed as decreased NADH over time, of recombinant purified LDHA at buffer pH 6.8, 7.2 and 7.5. Data are means of three separate measurements with two different protein preparations.

Fig. 3. Contributions to mitochondrial respiration and mitochondrial membrane potential. A. For HPDE and BxPC3 cells, OCR with inhibitors, each at 1 μM for pathways fueling mitochondrial respiration, including Etomoxir for FAO, BPTES for glutaminolysis, and UK5099 for the mitochondrial pyruvate carrier. Data are expressed as percent decrease relative to control OCR and are means ± s.e.m. of three cell preparations with statistical analysis by Student's Paired *t*-test. B. Representative confocal images of BxPC3 cells loaded with the methyl ester of the cationic dye tetramethylrhodamine that indicates mitochondrial membrane potential (Δψm) for control and with FCCP in the absence and presence of EIPA (10 μM). C. Quantification of tetramethylrhodamine staining expressed as control values relative to values with FCCP from five field-of-views in two cell preparations. Box plots show median, first and third quartile, with whiskers extending to observations within 1.5 times the interquartile range, and all individual data points.

Fig. 4. EIPA changes mitochondrial morphology. A. Imaris reconstructions of confocal images of the indicated cell types stained with Mitotracker DeepRed™ in the absence (control) or presence of EIPA (10 μM). Heat map of mitochondrial lengths and scale bar are included at bottom right. B-E For each indicated cell line, quantified mitochondrial lengths measured from confocal imagines using Nikon NIS software and binned using Excel software into four categories, 0-5 μm, 5-20 μm, 20-50 μm and > 50 μm, with data expressed as the number of mitochondrial structures within each category. Data are means ± s.e.m. of five fields of view from two cell preparations with statistical analysis by Student's Paired *t*-test.

Fig. 1. Manoli et al.

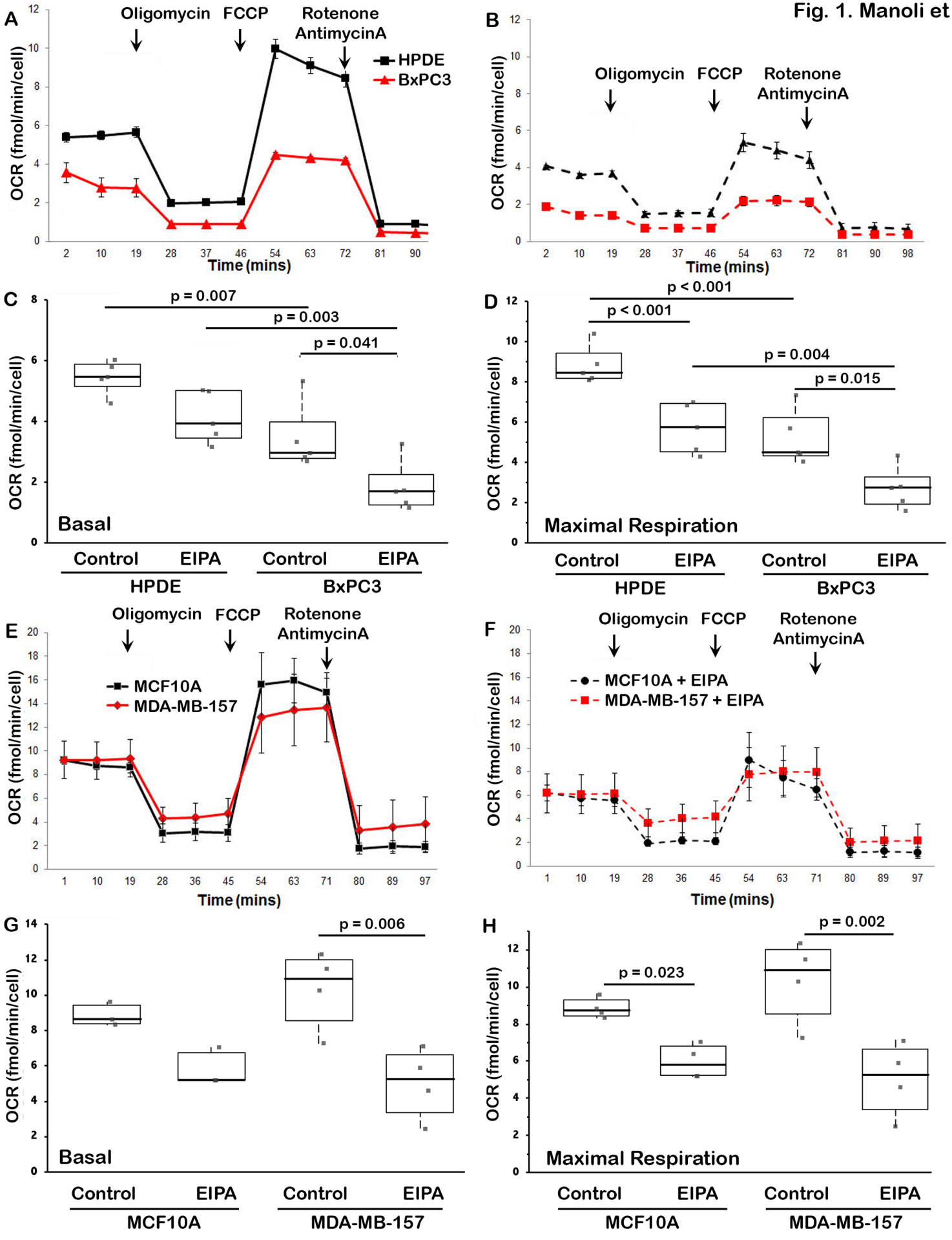

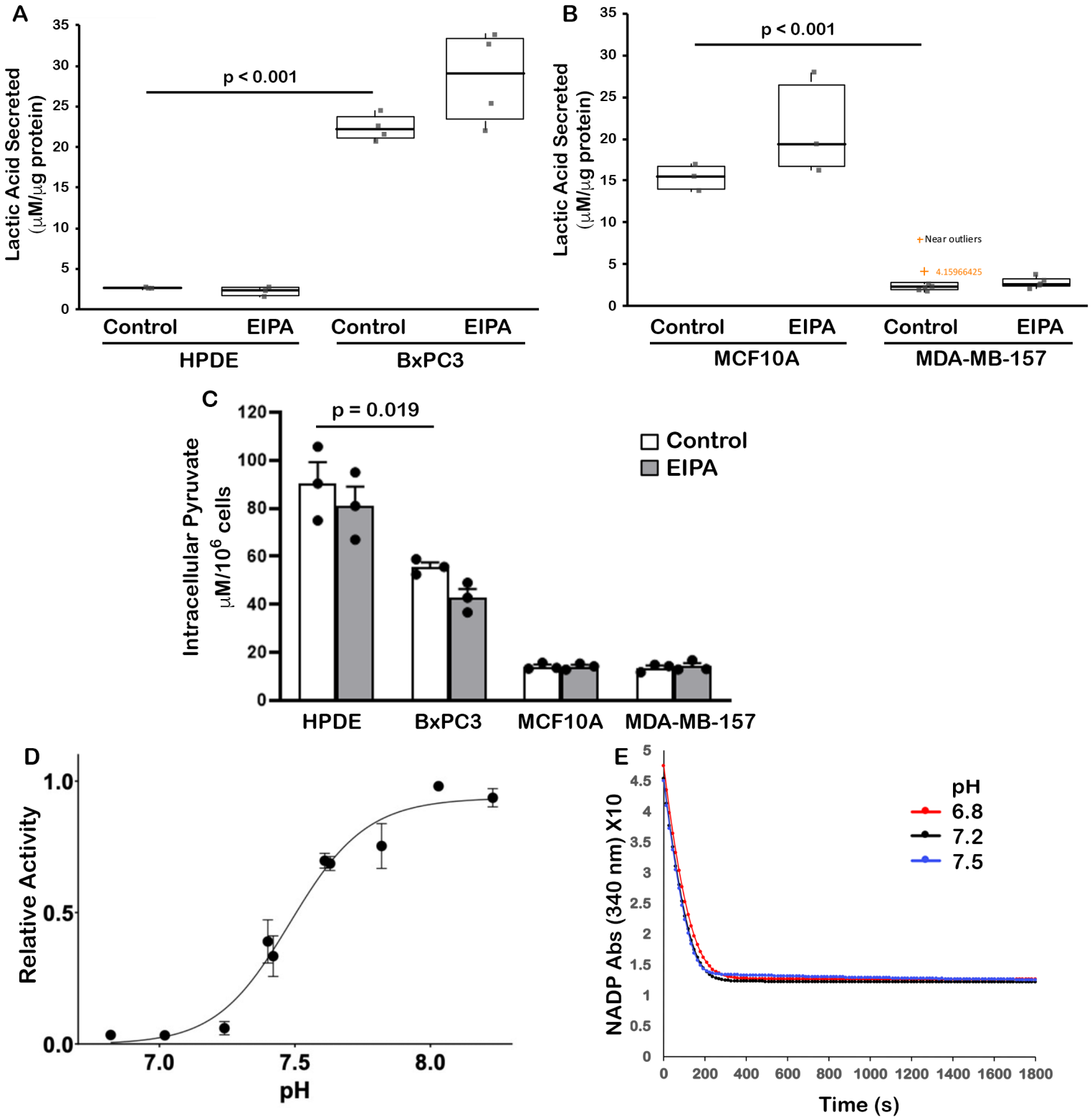

Fig. 2. Manoli et al.

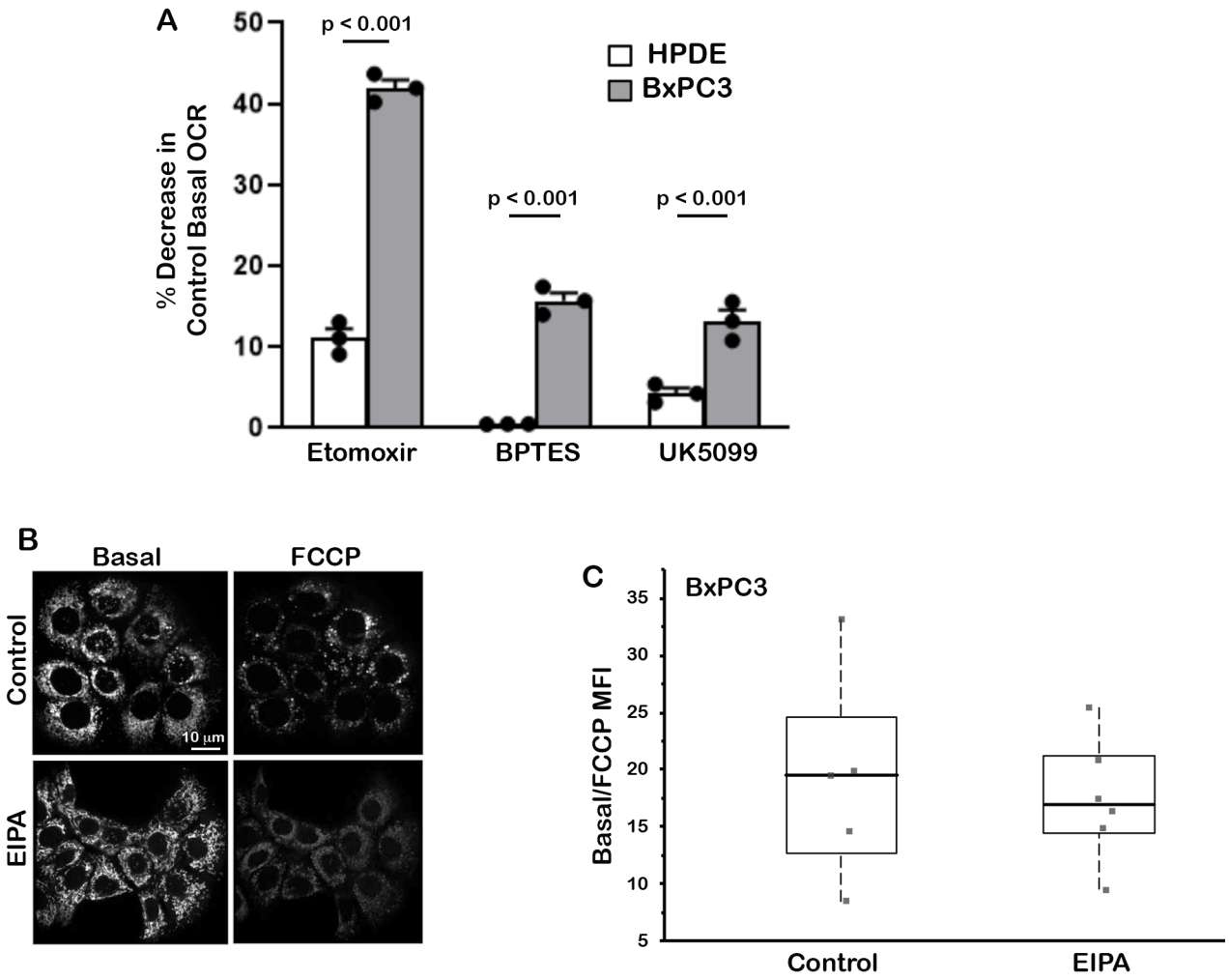
A
% Decrease in Control Basal OCR
50
40
30
20
10
0
p < 0.001
p < 0.001
p < 0.001
HPDE
BxPC3
Etomoxir
BPTES
UK5099
B
Basal
FCCP
Control
EIPA
10 μm
C
BxPC3
Basal/FCCP MFI
35
30
25
20
15
10
5
Control
EIPA

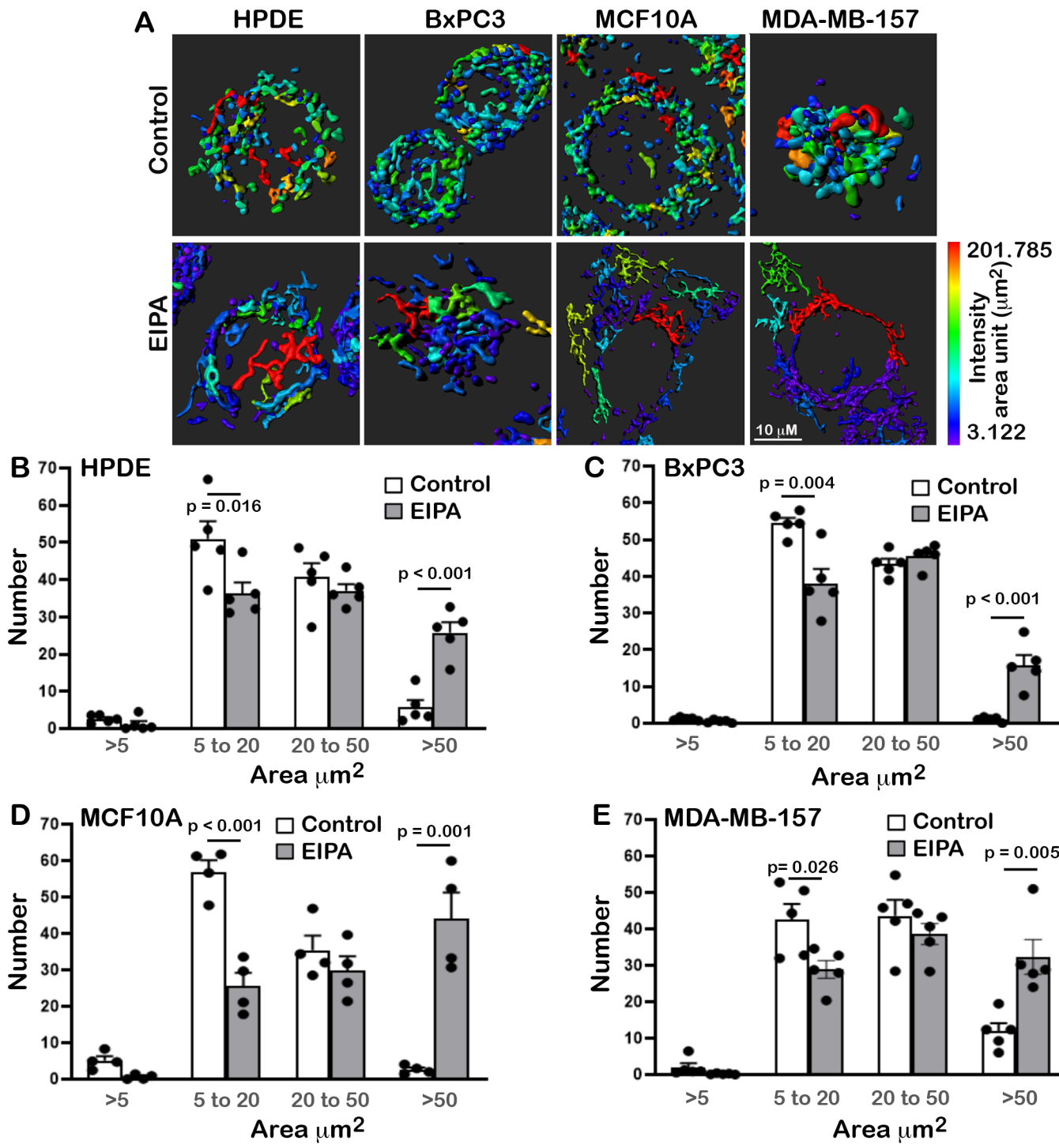

Fig. 4. Manoli et al.

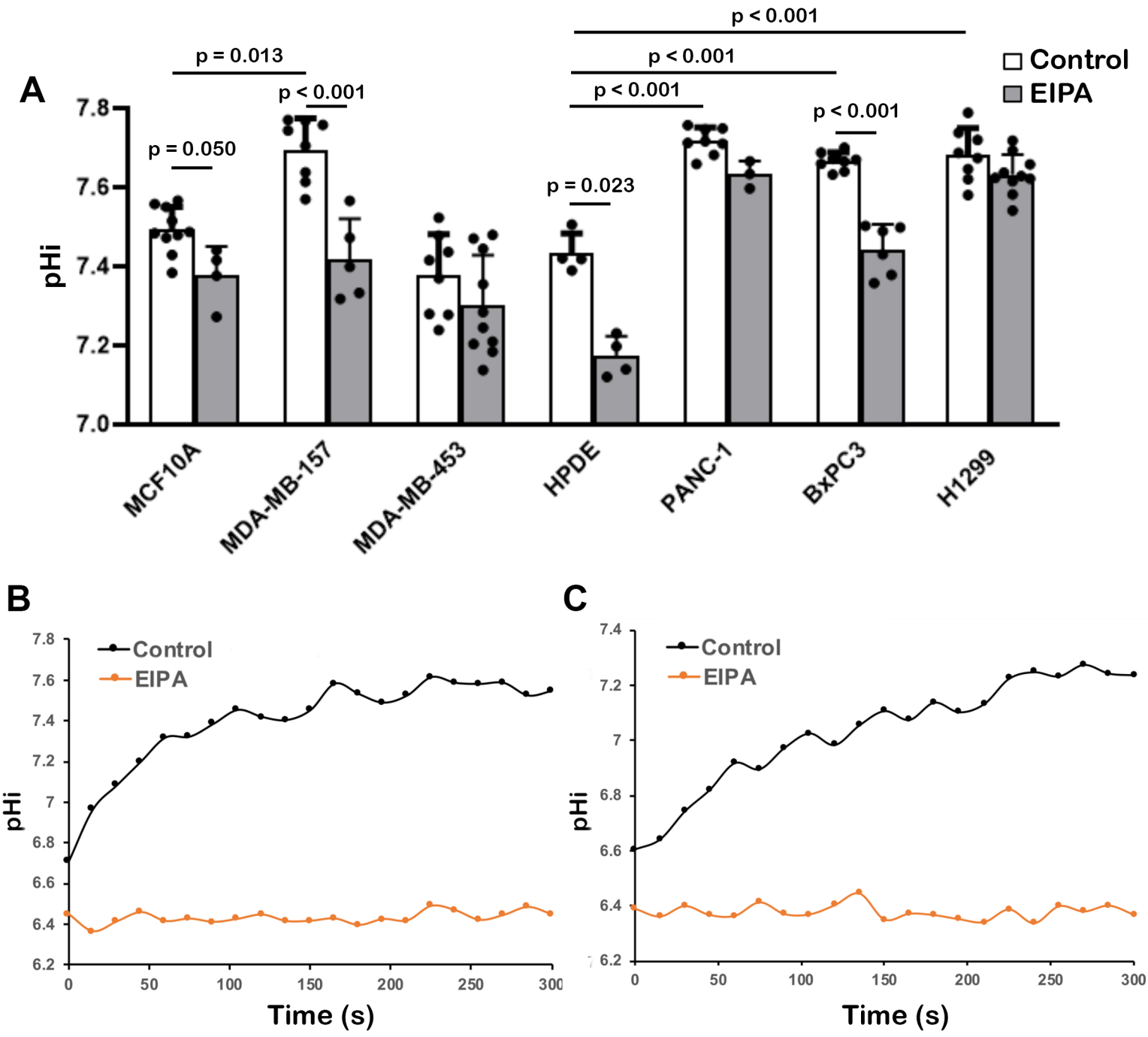

Manoli et al., Fig. S1

Fig. S2. Manoli et al.

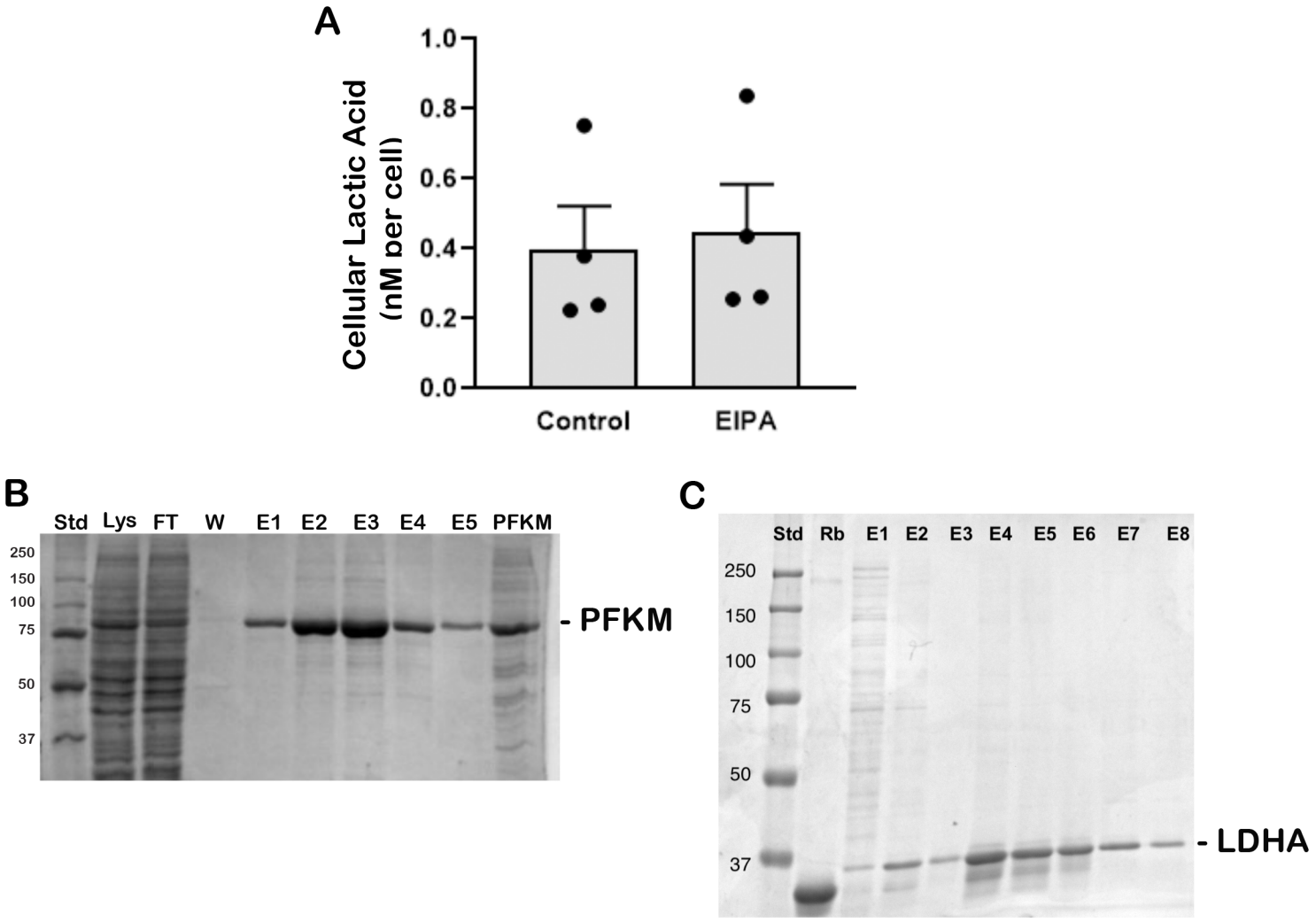

Fig. S3. Manoli et al.